Hindawi
Geofluids
Volume 2021, Article ID 4341804, 15 pages
https://doi.org/10.1155/2021/4341804

Research Article

Analyzing the Origin of Low Resistivity in Gas-Bearing Tight Sandstone Reservoir

Yanjiao Jiang[1,2] **Jian Zhou**[1,2] **Xiaofei Fu**[2,3] **Likai Cui**[2,3] **Chao Fang**[4] **and Jiangman Cui**[5]

[1]*School of Earth Sciences, Northeast Petroleum University, Daqing 163318, China*
[2]*State Key Laboratory Base of Unconventional Oil and Gas Accumulation and Development, Northeast Petroleum University, Daqing 163318, China*
[3]*Institute of Unconventional Oil & Gas, Northeast Petroleum University, Daqing 163318, China*
[4]*Production and Operation Department of the Sixth Oil Production Plant, PetroChina Daqing Oilfield Co., Ltd, Daqing 163114, China*
[5]*Technology Research Institute of Testing Company, PetroChina Dagang Oilfield Co., Ltd, Tianjin 300280, China*

Correspondence should be addressed to Yanjiao Jiang; jyjiao0224@163.com and Jian Zhou; zhouj87@163.com

Received 25 April 2021; Revised 24 June 2021; Accepted 7 August 2021; Published 31 August 2021

Academic Editor: Umberta Tinivella

Complex characteristics exist in the resistivity response of Gs reservoirs in the central inversion belt of the Xihu Sag, East China Sea Basin. Some drilling wells have confirmed the existence of abnormally low resistivity in gas reservoirs of the area; and the electrical logging response was unable to reflect fluid properties of the reservoir accurately. Therefore, it is necessary to analyze the origin of the low resistivity and determine its controlling factors. Based on experimental data of core analysis and numerical simulations of mud invasion, this study thoroughly explores the origin of low resistivity in the subject gas-bearing reservoir considering both internal and external factors. The results indicated that when there is no or a low degree of mud invasion, the fine lithology, complex pore structure, additional clay mineral conductivity, and high content of pyrite are the main internal factors driving the conditions present in the studied gas reservoir. When mud invasion occurs, the invasion of highly saline mud is the main external cause of low resistivity. The numerical simulation results indicated that a formation with good permeability and high overbalance pressure has a deep invasion depth. The resistivity around the well is obviously reduced after the invasion, and low resistivity would form easily. Combined with actual data of several wells, the main influencing factors of the reservoir's electrical characteristics were analyzed, and the main controlling factors of low resistivity in the gas reservoirs are given. This study provides valuable support for studying the low-contrast complex reservoir conductivity mechanism. The study also offers novel ideas for accurate calculation of saturation and the meticulous evaluation of reservoir for subsequent studies.

1. Introduction

Recent exploration and development efforts have indicated that the amount of hydrocarbon reserves in the low-resistivity reservoirs is considerable. Such reservoirs have been the research object of many studies, exhibiting the great potential of being complex reservoirs. Low-resistivity reservoirs are commonly found in most oilfields and have become one of the most valued sources to increase the production and tapping potential of old oilfields [1–4]. Many scholars have conducted in-depth research on the generation of low resistivity in these reservoirs [4–6]. The research results have indicated that the cause of the low resistivity could be classified into internal causes, external causes, and combined causes. The internal causes mainly include highly saline formation water, high irreducible water saturation formed by the development of micropores, additional conductivity of clay, conductive minerals in the rock skeleton, and thin

sand-shale interbedding. The external causes mainly include salty mud invasion and the limited detection range of the logging tools. Nevertheless, the simultaneous action of internal and external factors forms a combined cause. The identification and evaluation of low resistivity in the reservoir, which is an important issue in the field of logging [2, 7–10], have always been difficult. This is because the generation mechanism of low resistivity is complex and it differs in various oilfields, which introduces great difficulty to the interpretation of well logging data in every particular area [11–16].

The study area of this research is an important, large gas field in China discovered in 2013, with considerable reserves and favorable exploration and development prospects [17, 18]. The vertical heterogeneity of the target reservoir is strong, and a considerable part of the formation has low porosity and low permeability near a tight reservoir. The physical properties of the reservoir change greatly, and abnormally low-resistivity gas layers exist within many formations. Even in the same set of gas reservoirs, the resistivity exhibits obvious differences, which affects the accurate judgment of the gas-related reservoir properties. Many exploration wells have proved that some reservoir layers of the area have serious mud invasion, which distorts the response of electric logging. This kind of near-tight reservoir characteristics coupled with abnormally low resistivity bring great difficulties to the reservoir evaluation. At present, there is limited research on the origin of low resistivity in the gas reservoirs of the study area. Hence, it is necessary to carry out specific research to provide beneficial information for quantitative identification and effective development of low-resistivity reservoirs in this area.

Based on a large number of core experimental analysis data and numerical simulations of mud invasion, this paper thoroughly explores the origin of low resistivity in the subject tight sandstone gas reservoirs considering the internal and external factors. In this paper, theoretical analysis, numerical simulation, and data examples were combined to examine the main factors of the abnormally low resistivity and determine the potential of formations to represent low resistivity. Herein, detailed case analysis provided effective data for the accurate identification of low-resistivity reservoirs. This study provides a basis for further establishment of resistivity models for different generation mechanisms of low resistivity to improve the interpretation accuracy of the well logging data.

2. Study Area

The Xihu Sag is located at the northeast of the East China Sea Basin. It is a sedimentary sag filled with Cenozoic-aged sediments. The sag can be divided into five substructural units from west to east, including the western slope belt, western sag belt, central inversion structural belt, eastern sag belt, and eastern fault step belt [19]. The study area is located in the middle of the sedimentary sag (Figure 1), which is a key reservoir exploration area with high development value. In the study block, the Gs formation is a set of fluvial-lacustrine strata, and the sedimentary environment mainly consists of a fluvial delta system. The lithology of the Gs formation is complex, and mud intercalation and a small amount of glutenite are developed within a large set of sandstones [20, 21]. A considerable part of Gs formation is a tight sandstone reservoir. Table 1 shows the basic reservoir characteristics in Gs2-Gs4. As can be seen, there are some differences in sandstone body development, clay mineral content, and physical properties.

There is an obvious difference in the electrical properties of gas reservoirs in Gs2-Gs4 formation, ranging from 7 Ω·m to 70 Ω·m. The salinity of formation water is low, and the equivalent concentration of NaCl salt is approximately 6-10 g/L. As shown in Figure 2(a), No. 3 is a water layer, and its deep lateral resistivity response (RD) ≈ 7.5 Ω·m. The test results for layer No. 5 have proved it to be a gas layer, and its RD ≈ 12.5 Ω·m. The latter is a typical low-resistivity gas layer. In Figure 2(b), the upper layer (3561 m–3565 m) is mudstone and the average deep array lateral resistivity response (RLA5) ≈ 10 Ω·m, Nos. 38-40 are conventional gas layers, and the average RLA5 ≈ 50 Ω·m; the test results have indicated that Nos. 36-37 are gas layers and their average RLA5 ≈ 9 Ω·m. Nos. 36-37 are typical low-contrast gas layers.

In the study area, the differences between electric logging responses in some proven gas layers and the adjacent water layers are small, being even lower than the resistivity of water layers and mudstone layers. The appearance of low-resistivity gas layers introduces difficulties to well logging interpretation jobs. Therefore, it is necessary to analyze the main controlling factors from the viewpoint of the internal and external factors.

3. Analyzing Internal Factors

Combining the core analysis, logging, and testing data of the subject formations, we analyzed the internal causes of low resistivity from different aspects including lithology, pore structure, and mineral composition.

3.1. Fine Lithology. The thin-section analysis and rock particle size experimental data of the low-resistivity layers indicated that the lithology is mainly fine sandstone, and the grain size of the rock is relatively fine (as shown in Figure 3). The median grain size of the low resistivity-gas layer is mainly distributed in the range of 0.1-0.3 mm, and for the conventional gas layer is 0.2-0.5 mm (as shown in Figure 4). Fine rock particles, on the one hand, cause the film adsorbed on the particle surface to retain more water. On the other hand, the tortuosity of pores increases the proportion of microcapillary pores, which increases the content of retained capillary water. These factors lead to an increase in immobile water saturation. The higher the immobile water saturation is, the easier it is to form a good ionic conductive network in the reservoir, and it is easier to form a low-resistivity gas reservoir. Fine lithology is one of the main factors that lead to low resistivity in the gas reservoirs. This feature is more significant in Gs2 formation, where the content of fine sandstone is 90%, and the main distribution range of micropores is 30%-42%. The resistivity of the gas-bearing layer is generally low.

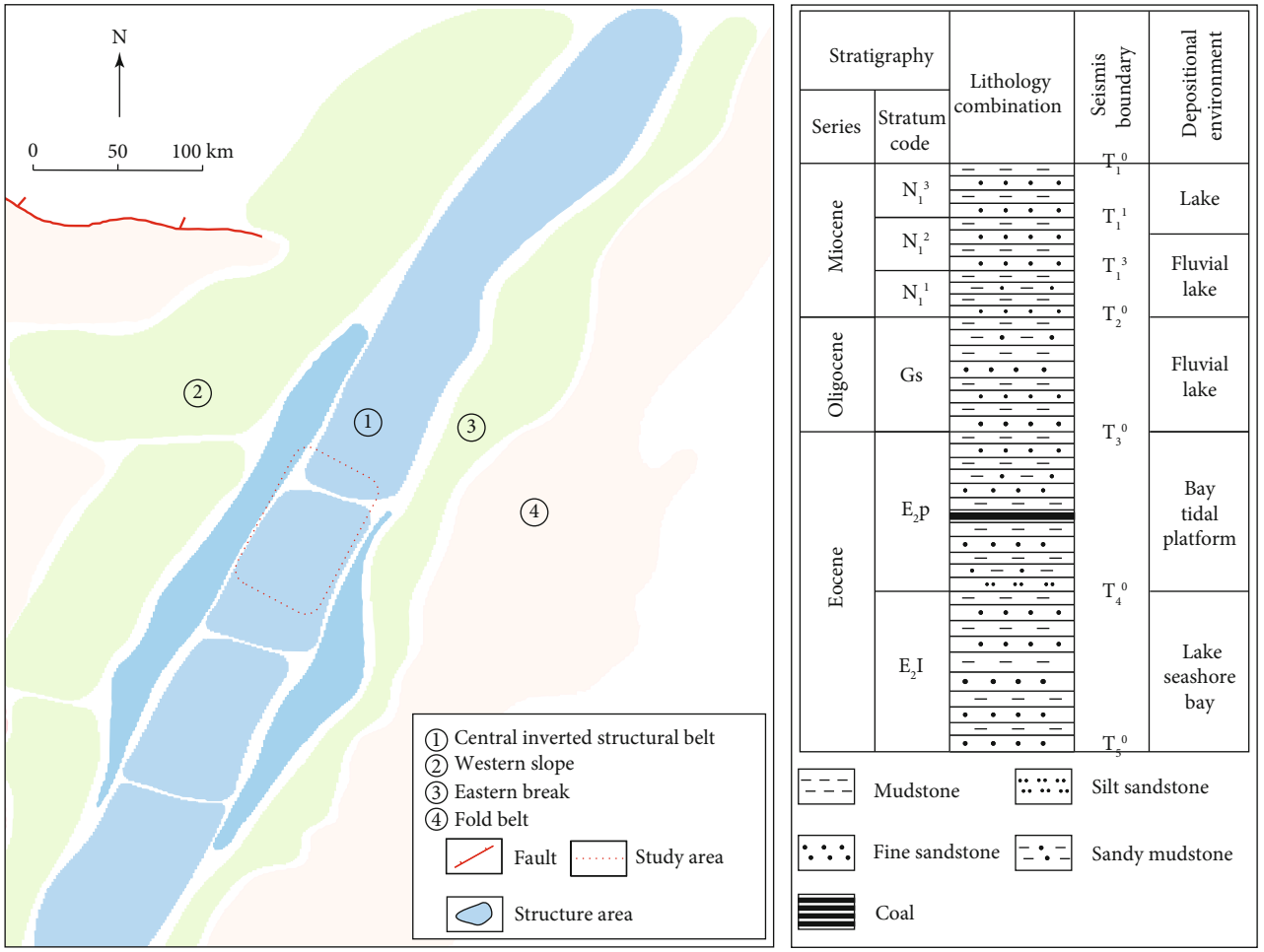

Figure 1: Regional position and stratigraphic column of the central inversion structural belt in the Xihu Sag.

Table 1: Statistics of basic reservoir characteristics.

Stratum	Sandstone	Lithology	Physical property		
		Rock type	Clay mineral (%)	Porosity (%)	Permeability (mD)
Gs2	Thin sandbody development	Mainly fine sandstone, single lithology	6-10	8-16	0.1-3
Gs3	Thick sandbody development	Mainly fine sandstone, complex lithology, little pebbled sandstone	2-8	8-12	0.3-3
Gs4	Thick sandbody development	Mainly fine sandstone, complex lithology	2-8	4-12	0.1-3

3.2. Additional Conductivity of Clay Minerals. The experimental results for the clay mineral composition analysis showed that the content of clay minerals in the low-resistivity gas reservoir of the area is relatively high, with the main distribution range of 6-16%. However, the content of clay minerals in the conventional gas layer is relatively low, with the main distribution range of 3-8%. The clay minerals mostly include illite-montmorillonite mixed layer, chlorite as the second abundant clay, and kaolinite with the least amount. The average content of the illite-montmorillonite mixed layer is higher than that of other minerals in the low-resistivity gas reservoir. The illite-montmorillonite mixed layer has a higher cation exchange capacity, and its additional conductivity is the fundamental reason for the reduction in the formation resistivity [22, 23]. For the distribution form of the clay minerals, it can be seen from the thin sections that the clay minerals mostly appear in parallel layers or fill in the pores among the rock particles in fibrous form or are attached to the surface of rock particles in thin-film form (as shown in Figure 5).

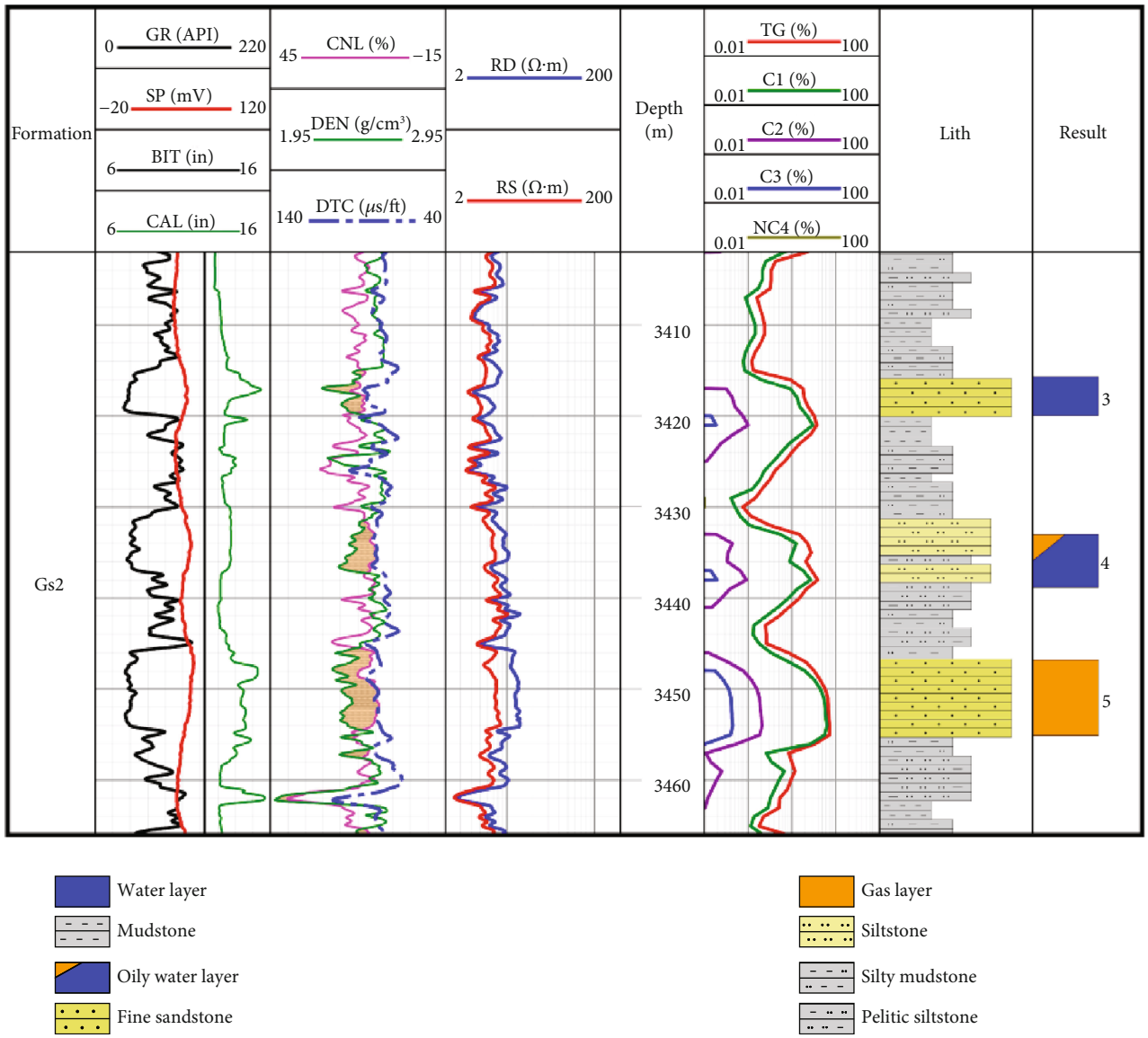

(a)

Figure 2: Continued.

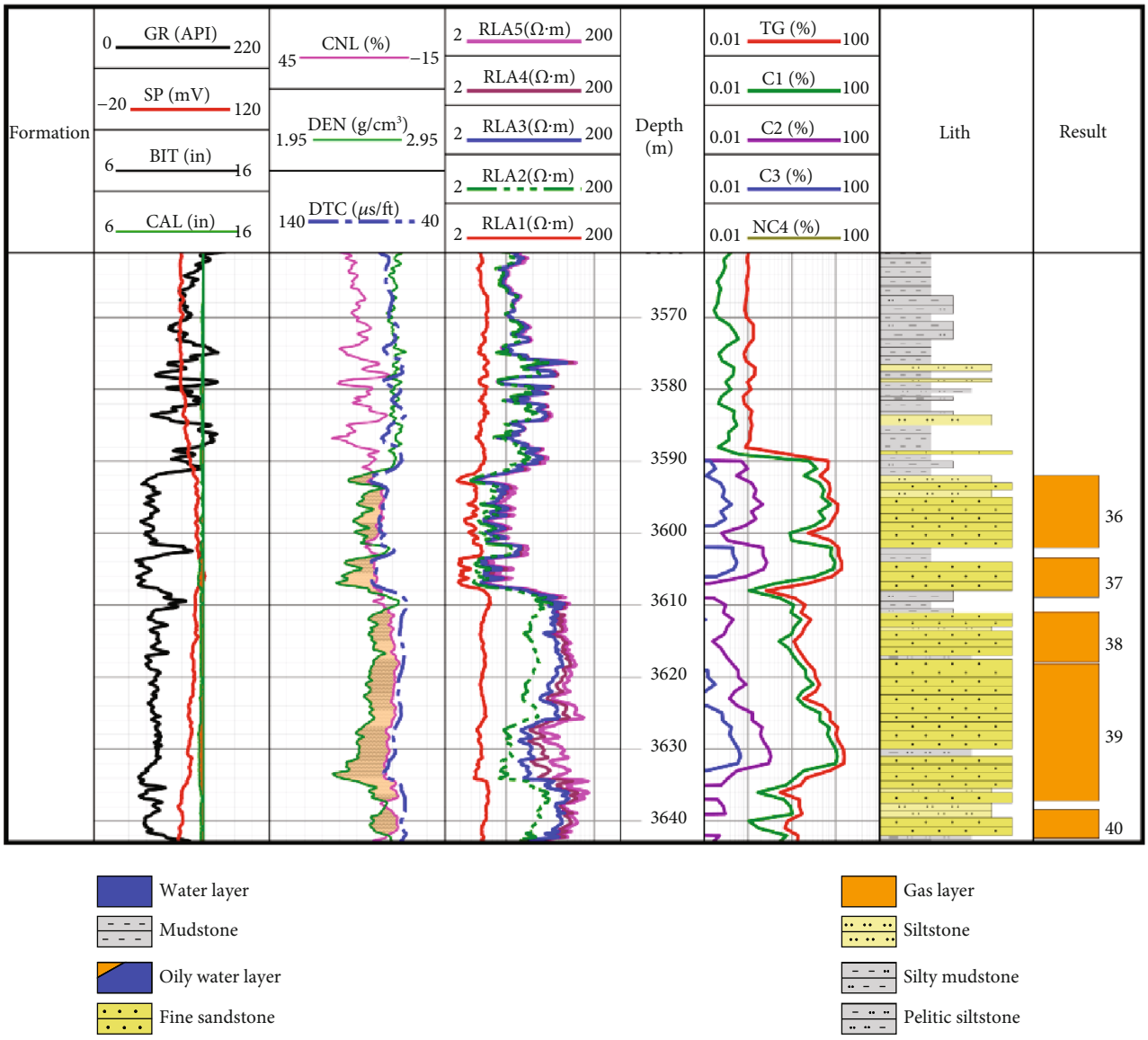

(b)

Figure 2: Comprehensive logging map of Gs formation: (a) X-B-1 well and (b) X-A-1 well.

These distribution forms effectively improve the electrical conductivity network, reduce the reservoir resistivity, and form low-resistivity gas reservoirs. High clay content and conductive distribution form are the main reasons for many low-resistivity reservoirs.

3.3. Complex Pore Structure. The studied formation is deeply buried at more than 3000 m. Due to the influence of the sedimentary environment, diagenesis, and rock particle sorting, the pore structure of the reservoir is complex. According to observation of a scanning electron microscope (SEM), the proportion of intragranular pores is higher in certain low-resistivity layers. A comparison of mercury injection curves showed that the capillary pressure of conventional gas reservoir is characterized by a coarse skewness and a low displacement pressure (P_d), while the low-resistivity gas reservoir is characterized by medium-fine skewness and a relatively high displacement pressure (as shown in Figure 6). The complex pore structure increases the capillary displacement pressure. Herein, the pore throat seepage ability is poor, and a part of the formation water remains in the micropores, which increases the immobile water saturation and forms a low-resistivity gas reservoir [24, 25].

3.4. High Content of Conductive Minerals. Conductive minerals (such as pyrite and magnetite) have low resistivity. When conductive minerals exist in clastic particles or are filled within the rock skeleton, their presence influences the rock's conductivity [26, 27]. It has been proved that there are low-resistivity gas layers in Gs3 formation in many wells. And a large amount of pyrite was found in the sidewall core analysis data. X-ray diffraction analysis showed that the pyrite content of the heavy minerals is 6-8%, which is evidently higher than that of the adjacent sandstone layer.

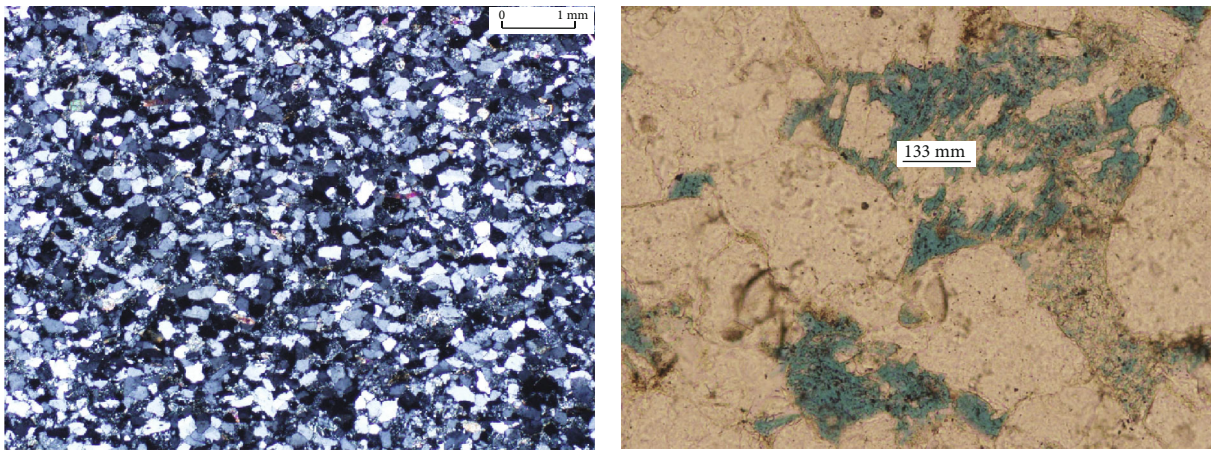

Figure 3: Thin sections of low-resistivity rocks: (a) fine rock particles, X-A-1, 3431 m; (b) crumb solution pores, X-B-1, 3455 m.

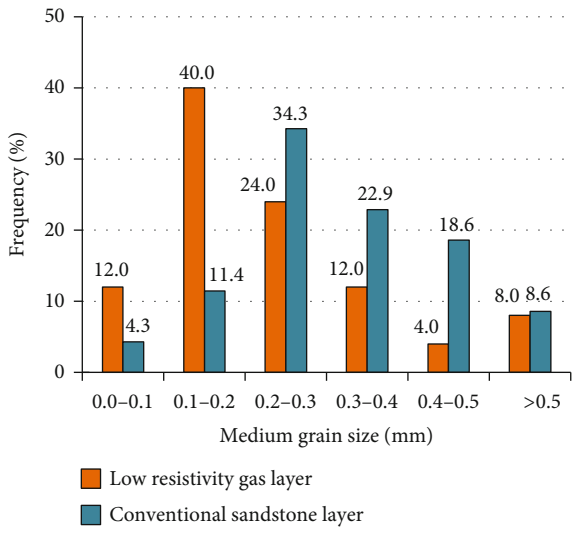

Figure 4: Frequency distribution histograms of medium grain size.

When a certain amount of conductive minerals exists in the formation and contact with the other conductive components, they easily form a connected conductive path, which has a substantial impact on reducing rock resistivity [28–30]. In addition, according to thin section scanning photos, the heavy minerals exist in the form of layered and banded enrichment (as shown in Figure 7), indicating that the distribution forms of high-conductivity minerals also have a crucial influence on reducing rock resistivity.

4. Analyzing External Factors

This section mainly analyzes the external causes of low resistivity from the viewpoint of well logging tasks and focuses on the impact of mud invasion on the formation resistivity at different mud invasion conditions. The study area is an offshore oilfield. Several wells have confirmed that there is a serious mud invasion phenomenon in the target formation. There are considerable differences in mud invasion in different conditions, which have a notable impact on the electrical logging response. Based on the actual data of reservoir characteristics and fluid properties, the formation model was constructed and the formations prone to mud invasion were determined.

A limited-size 3D single well formation model was established to simulate the mud invasion process by using reservoir numerical simulation technology [31–34]. Figure 8 shows the diagram of the mud invasion occurrence model. The radial distribution of water saturation and salinity under different invasion conditions was obtained by simulation, and then, the dynamic change in the formation resistivity around the wellbore was obtained by Archie equation [35] assuming two-phase formation fluids, i.e., gas-water. The fluid seepage process followed the mass balance equation, and the mixture of drilling fluid and the original formation water followed the convection-diffusion equation [34]. According to the actual physical properties, fluid characteristics, Archie's equation parameters, and dynamic test data of the target area, the basic parameters of the numerical simulation model were selected as shown in Table 2. This part focuses on the influence of overbalance pressure, formation permeability, and mud filtrate salinity during the invasion. The ranges of simulated parameters were determined by the measured and core analysis data of the target area.

4.1. Influence of Overbalance Pressure. According to test data, the main range of overbalance pressure is mainly 1 MPa-8 MPa. The simulation conditions employed in this study were as follows: $K = 1$ mD, $\varphi = 0.085$, $S_w = 0.3$, $C_{mf} = 60000$ ppm, and $C_w = 10000$ ppm. The invasion occurrence model was divided into three layers, and $\triangle P$ was set to 2 MPa, 3.5 MPa, and 7 MPa. ($\triangle P$: overbalance pressure.)

Figure 9 shows the radial distribution of formation water salinity, water saturation, and formation resistivity under different overbalance pressures when the invasion time $t = 2$ d. The abscissa is the distance from the wellbore. When the overbalance pressure is larger, the velocity of mud filtrate is larger, and the volume of mud filtrate entering the

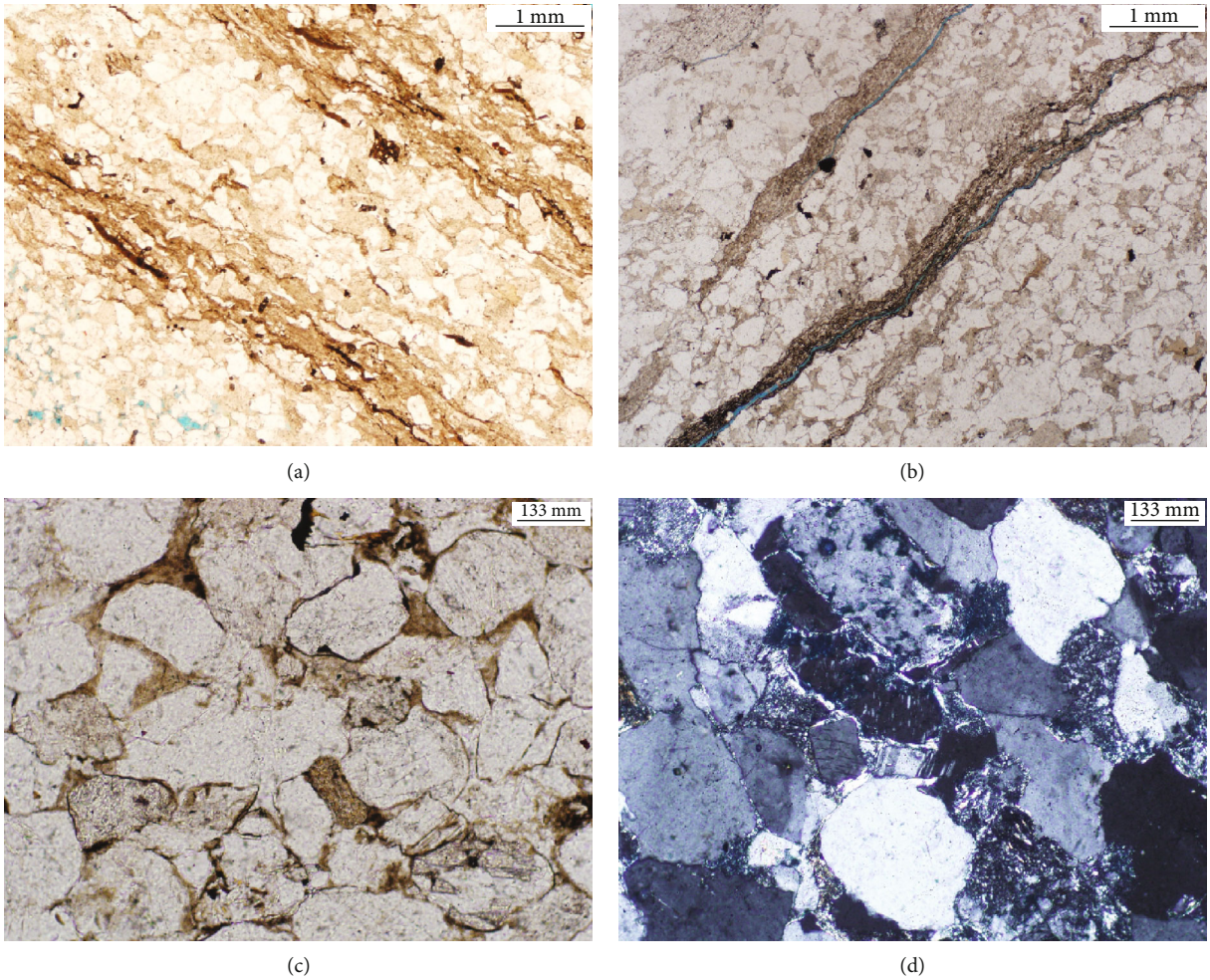

Figure 5: Thin sections to study the clay minerals' distribution form: (a) parallel layer enrichment, X-B-3, 3567 m; (b) banded enrichment, X-A-2, 3962.1 m; (c) thin-film form, X-A-2, 3640 m; (d) fibroid form X-A-1, 3446 m.

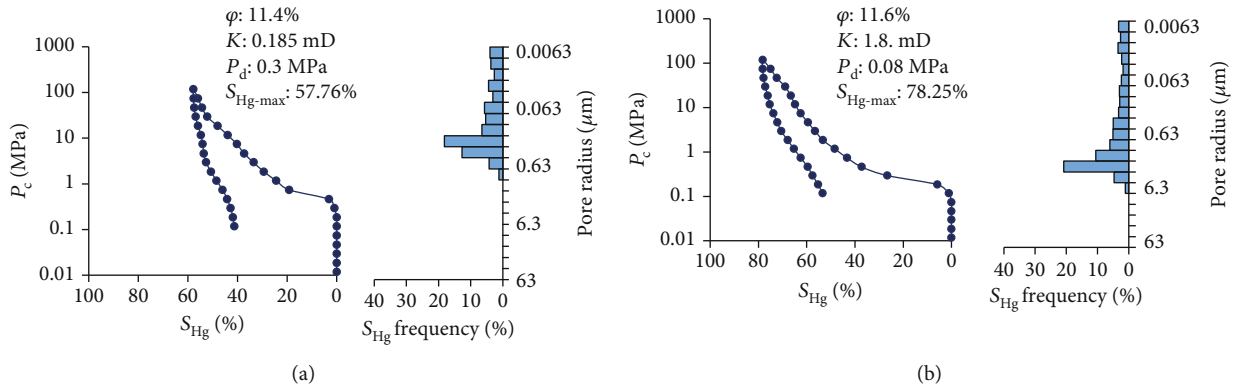

Figure 6: Mercury injection curve of low-resistivity gas layer and conventional gas layer: (a) low-resistivity gas layer and (b) conventional gas layer.

formation is larger, which leads to deeper mud invasion. Due to the invasion of high salinity mud filtrate, the water salinity and water saturation of the invasion zone increase significantly, resulting in a substantial decrease in the resistivity near the wellbore. In this case, the formation resistivity near the wellbore decreased to 4 Ω·m after the invasion, while the original formation resistivity was 115 Ω·m (as shown in Figure 9(c)). Therefore, a low-resistivity profile would appear under invasion of a high-salinity mud.

4.2. Influence of Permeability. According to the core analysis data, the main distribution range of formation permeability

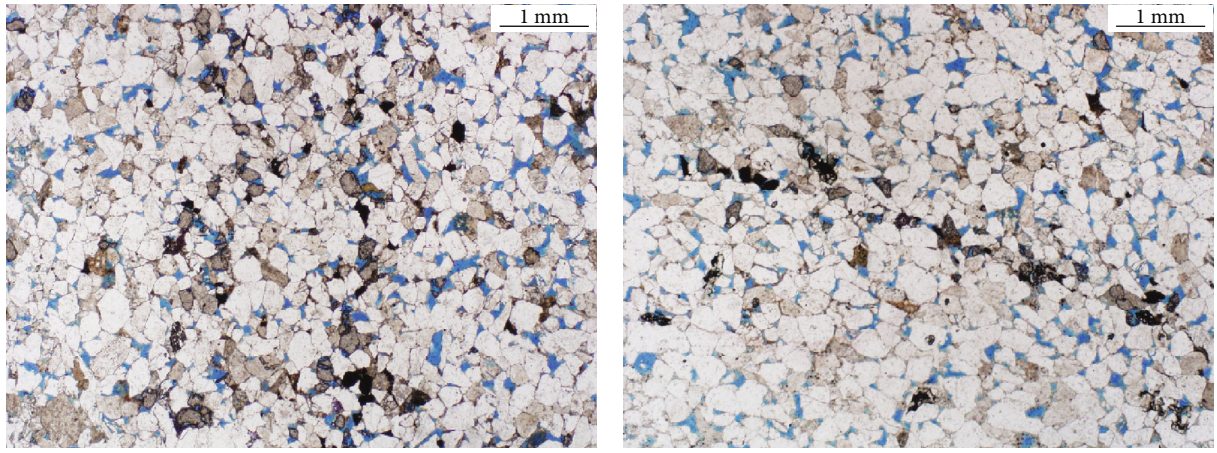

(a) (b)

Figure 7: Thin sections of conductive minerals' distribution form: (a) enrichment, X-A-1, 3603 m; (b) banded enrichment, X-A-1, 3604.5 m.

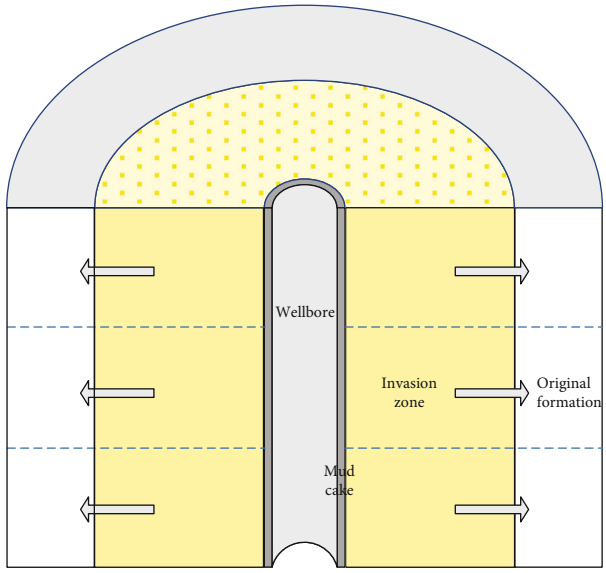

Figure 8: The schematic model of mud invasion.

Table 2: Basic parameters used in mud filtrate invasion model.

	Parameter	Value
Fluid properties	Water density (g/cm^3)	1.05
	Gas density (g/cm^3)	0.018
	Water viscosity (cp)	0.42
	Gas viscosity (cp)	0.024
	Water compressibility (psi^{-1})	5.8×10^{-6}
	Formation water salinity (C_w, ppm)	10000
	Mud filtrate salinity (C_{mf}, ppm)	60000
Reservoir properties	Rock compressibility (psi^{-1})	4.3×10^{-6}
	Formation permeability (K, mD)	1
	Formation porosity (φ)	0.085
	Formation temperature (°C)	122
	Formation initial water saturation (S_w)	0.3
	Irreducible water saturation	0.15
	Residual gas saturation	0.15
Archie equation	Cementation exponent, m	1.87
	Saturation exponent, n	1.71
	Lithology factor, a	1

is 0.1 mD-10 mD, and the relationship between porosity and permeability follows $K = 0.0072e^{58.231\varphi}$. The simulation conditions employed in this part were as follows: $\triangle P = 3.5$ MPa, $S_w = 0.3$, $C_{mf} = 60000$ ppm, and $C_w = 10000$ ppm. The invasion occurrence model was divided into five layers with formation permeability values of 0.1 mD, 0.5 mD, 1 mD, 5 mD, and 10 mD. Based on the regression equation, the corresponding formation porosity was 0.045, 0.073, 0.085, 0.111, and 0.125.

Figure 10 shows the radial distribution of formation water salinity, water saturation, and formation resistivity around the wellbore for the different values of the formation permeability when the invasion time $t = 2$ d. The mud invasion depth increases with increasing formation permeability, and the amount of increase is larger when $K > 1$ mD. The simulation results showed that for the nearly tight sandstone gas reservoir, the better physical properties of the formation leads to the greater mud invasion depth and a larger resistivity variation range. Therefore, in gas reservoirs with good physical property, the mud invasion depth is generally high, and the electric logging response is often distorted. The invasion of highly saline mud makes it difficult to identify the electrical characteristics of the original formation by electric logging response.

4.3. Influence of Mud Filtrate Salinity. According to water analysis data, the formation water salinity is mainly 5000 ppm-14000 ppm, and the mud filtrate salinity is mainly 35000 ppm-50000 ppm. The simulation conditions employed

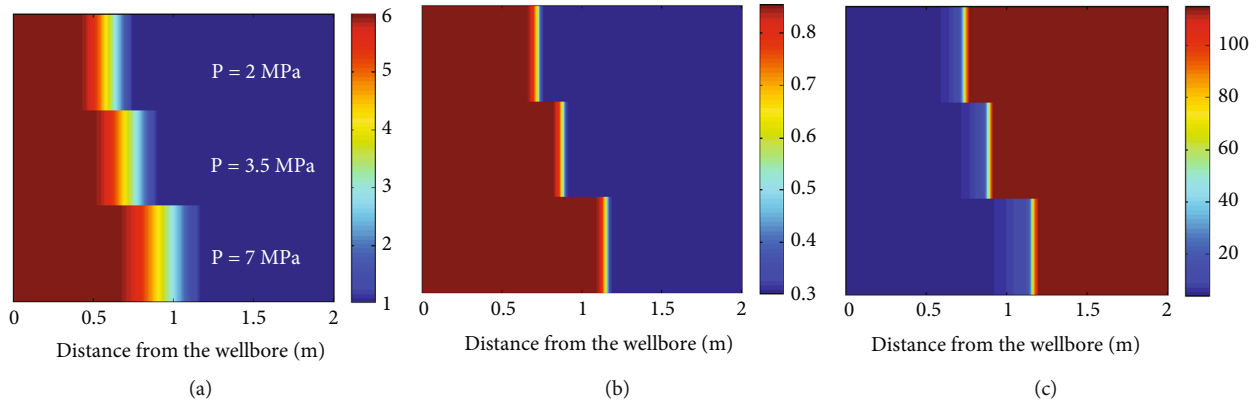

Figure 9: Radial invasion profile for variations in the overbalance pressure: (a) salinity distribution profile, $\times 10^4$ppm; (b) water saturation distribution profile, f; (c) formation resistivity distribution profile, Ω·m.

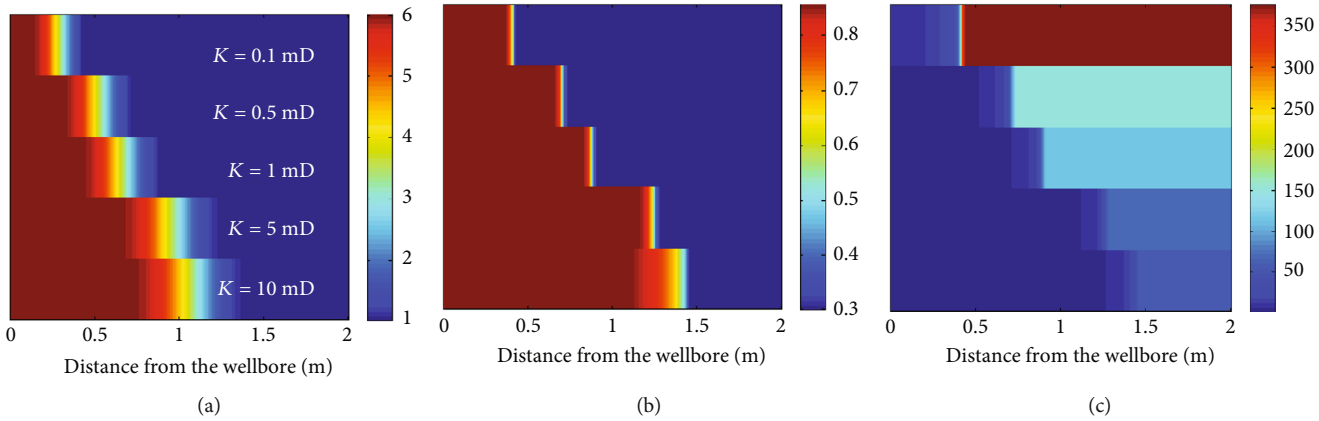

Figure 10: Radial invasion profile for variable formation permeability values: (a) salinity distribution profile, $\times 10^4$ppm; (b) water saturation distribution profile, f; (c) formation resistivity distribution profile, Ω·m.

in this part were as follows: $\triangle P = 3.5$ MPa, $K = 1$ mD, $\varphi = 0.085$, $S_w = 0.3$, and $C_w = 10000$ ppm. The invasion formation model was divided into five layers, and C_{mf}/C_w ratios were set to 0.1, 0.5, 1, 3, and 6.

Figure 11 shows the radial distribution of formation water salinity, water saturation, and formation resistivity around wellbore under different mud filtrate salinities when the invasion time $t = 2$ d. The salinity of mud filtrate has no obvious influence on the invasion front. With the increasing salinity of mud filtrate, the invasion depth is nearly constant. In Figure 11(c), it can be seen that the C_{mf}/C_w value has a great influence on the formation resistivity of the invasion zone. When $C_{mf}/C_w \geq 1$, the formation exhibits an obvious low invasion profile, and the resistivity of the invasion zone is obviously lower than that of the original formation. When $C_{mf}/C_w < 1$, an obvious "low-resistivity ring" appears. For the study area, the C_{mf}/C_w value is generally higher than 4. Therefore, with other conditions in a certain case, saline mud filtrate is an important factor to reduce the formation resistivity of the invasion zone.

4.4. Array Laterolog Response and Mud Invasion. Array laterolog can provide five resistivity curves with different detection depths. Compared with the conventional dual laterolog, array laterolog has a higher vertical resolution and provides more radial resistivity information [35–37]. In order to thoroughly analyze the relationship between mud invasion and array laterolog response, we carried out the numerical simulation of mud invasion in actual formations.

Taking X-B-2 well as an example, 42 sublayers were selected at the depth of 3740-3781 m. The basic simulation parameters were determined according to the core experimental data and the measured data of the formation, and the gravitational differentiation between layers was considered in the simulation. The simulated mud invasion time was 7 d, considering that the time from drilling to logging is approximately 7 d, and the invasion depth and invasion zone resistivity were obtained. The finite element forward model [38, 39] was applied to calculate the array lateralog responses of the simulation area [40–42]. In Figure 12, the fifth track is the comparison between the measured and simulated value of array lateralog responses. The data of calculated values and the measured values are shown in Table 3. RLA1, RLA2, RLA3, RLA4, and RLA5 represent the apparent resistivity from shallow to deep, respectively. As can be seen from the comparison results, the calculated values coincide with the measured values and the relative errors are very small. The results verified the accuracy of the reservoir

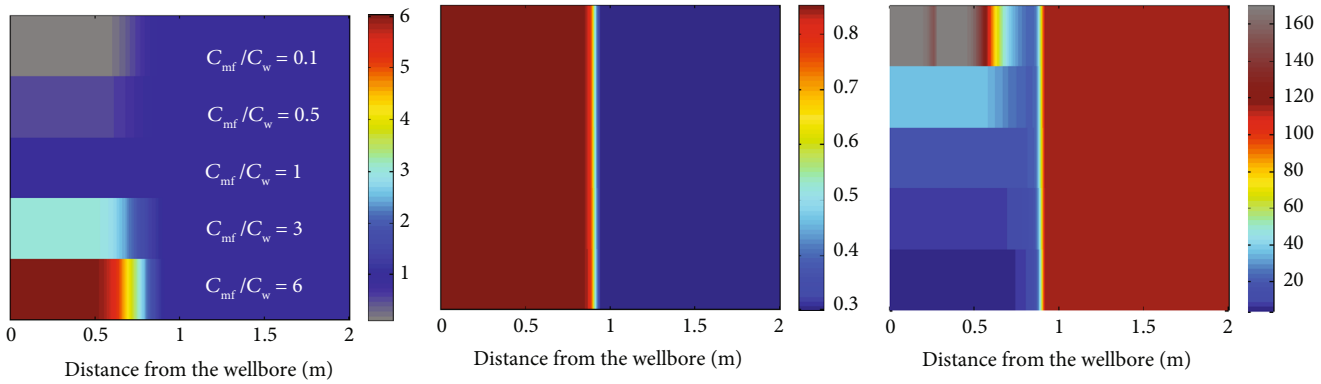

Figure 11: Radial invasion profile for variations in the mud filtrate salinity: (a) salinity distribution profile, $\times 10^4$ppm; (b) water saturation distribution profile, f; (c) formation resistivity distribution profile, Ω·m.

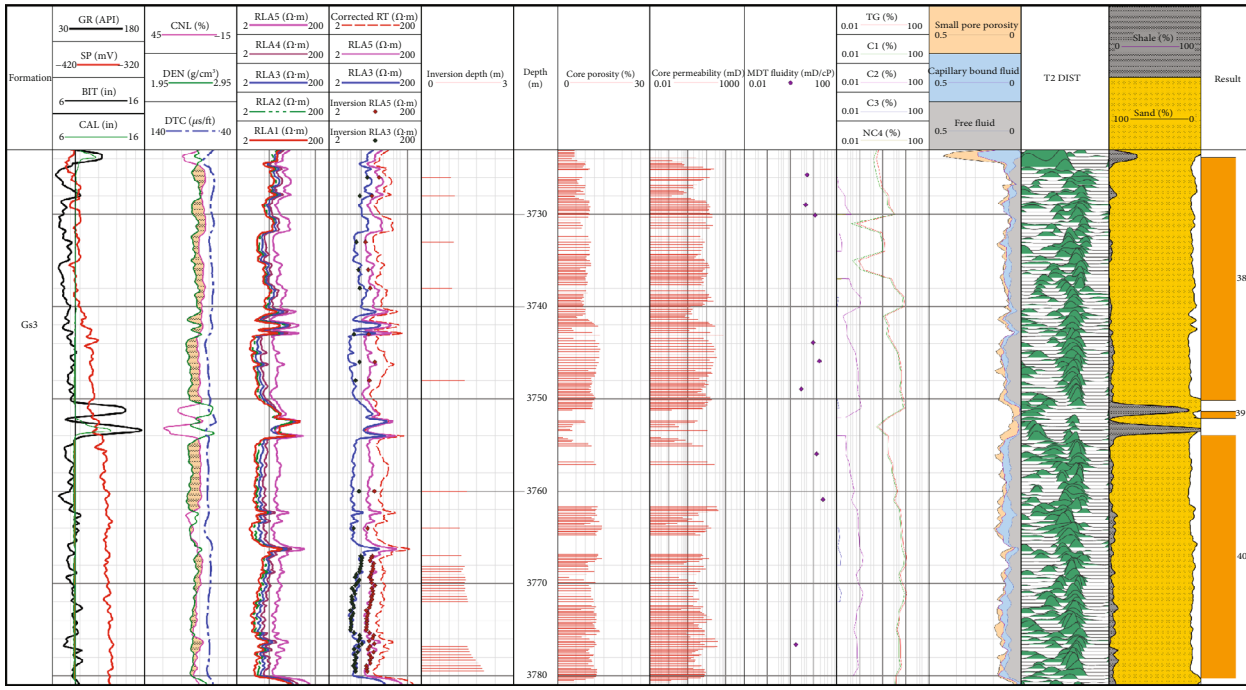

Figure 12: The analysis diagram of mud invasion simulation results in well X-B-2.

numerical simulation method. In Figure 12, the sixth track is the simulated invasion depth. The results show that serious mud invasion occurred in this section, and the better the formation physical property was, the deeper the mud invasion was. The invasion zone resistivity decreases greatly due to highly saline mud invasion. The array laterolog response is significantly lower than that of the original formation at deeper invasion depths. As the depth increases, the array laterolog curves with different detection depths show different amounts of decrease. The curve of shallow detection depth is affected more significantly. The gas layers presented low resistivity due to the invasion of high salinity mud, which was not a real electrical reflection but rather an illusion of the "low resistivity".

Mud invasion affects the array laterolog response directly. For reservoir interpretation and evaluation, the low resistivity caused by high salinity mud invasion should be considered. The analysis of mud invasion and the response characteristics of the array has great importance for identifying effective reservoirs and improving the accuracy of interpretation.

5. Case Study Analysis and Discussion

In order to determine the main controlling factors of low resistivity, the typical causes of low resistivity including the internal, external, and combined causes were selected, respectively. Detailed physical properties, mineral composition, and mud

Table 3: Calculated and measured values of the array laterolog response for well X-B-2.

Layer number	Depth (m)	Calculated results					Measured results				
		RLA1 (Ω·m)	RLA2 (Ω·m)	RLA3 (Ω·m)	RLA4 (Ω·m)	RLA5 (Ω·m)	RLA1 (Ω·m)	RLA2 (Ω·m)	RLA3 (Ω·m)	RLA4 (Ω·m)	RLA5 (Ω·m)
1	3767.2	7.06	8.68	10.35	12.41	16.52	7.27	8.38	9.80	11.18	17.59
2	3767.5	6.28	7.70	10.03	10.93	15.52	7.32	8.34	9.94	11.84	18.19
3	3767.8	7.96	8.65	9.94	11.40	18.68	7.22	8.04	9.72	11.92	18.37
4	3768.1	7.86	9.54	9.85	10.65	17.57	7.76	8.74	10.44	12.94	20.54
5	3768.4	6.92	8.19	9.39	11.35	18.01	6.60	7.45	8.64	10.52	17.19
6	3768.7	7.49	7.80	9.12	10.53	16.77	6.55	7.29	8.40	10.11	16.83
……	……	……	……	……	……	……	……	……	……	……	……
37	3778.0	5.47	6.15	7.66	10.84	16.61	5.66	6.48	7.99	10.59	15.72
38	3778.3	5.34	5.90	7.23	9.09	15.36	4.92	5.77	7.43	9.73	13.54
39	3778.6	5.51	6.07	7.43	9.32	15.70	5.02	6.17	7.93	9.59	13.34
40	3778.9	4.73	5.35	6.71	8.14	12.91	4.75	5.87	6.90	7.99	11.72
41	3779.2	5.13	6.39	7.44	9.12	13.04	4.94	5.65	6.55	7.68	12.05
42	3779.5	5.57	7.28	7.50	8.27	13.46	5.87	6.67	7.94	9.71	15.98
Average relative error (%)							7.61	7.93	6.08	8.92	8.77

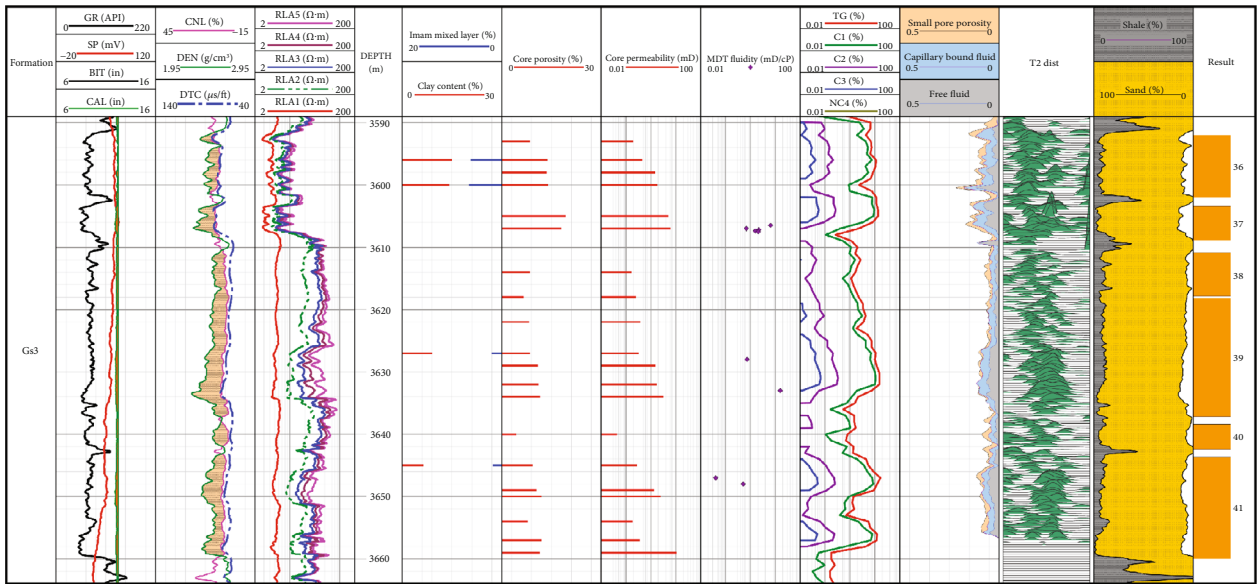

Figure 13: Log data diagram of Gs3 in X-A-1.

invasion data implemented during analysis will be provided in the upcoming sections.

5.1. Internal Cause. Figure 13 represents the log interpretation results of well X-A-1. At depths of 3591-3608 m, the resistivity is approximately 7-15 Ω·m. Pure gas samples were successfully obtained through the wireline formation test at 3606.5 m, and the content of C1 was 84%, confirming the presence of a gas layer. The resistivity of the upper low-resistivity gas reservoir is quite different from that of the lower conventional gas reservoir. X-ray diffraction analysis showed that a large amount of pyrite can be found in the cores obtained from 3598 to 3608 m, and the pyrite content was 7-8%, which is noticeably higher than that of the lower sandstone body. In addition, the clay content of the upper reservoir was 15.1%, which is higher than that of the lower conventional gas reservoir (8.0%). The relative content of the illite-montmorillonite mixed layer in the clay reached as high as 46%. The thin section and imaging logging data showed that the clay is mostly layered and banded. There was no obvious difference in physical properties and pore radius distribution of the zones. Comprehensive analysis revealed that there are two main explanations for this low-resistivity layer. First, the high content of pyrite makes the rock extremely conductive and reduces reservoir resistivity. Second, the high content of clay and the conductive distribution form effectively enhance the rock's conductivity. The small-amplitude difference of the array laterolog curve in

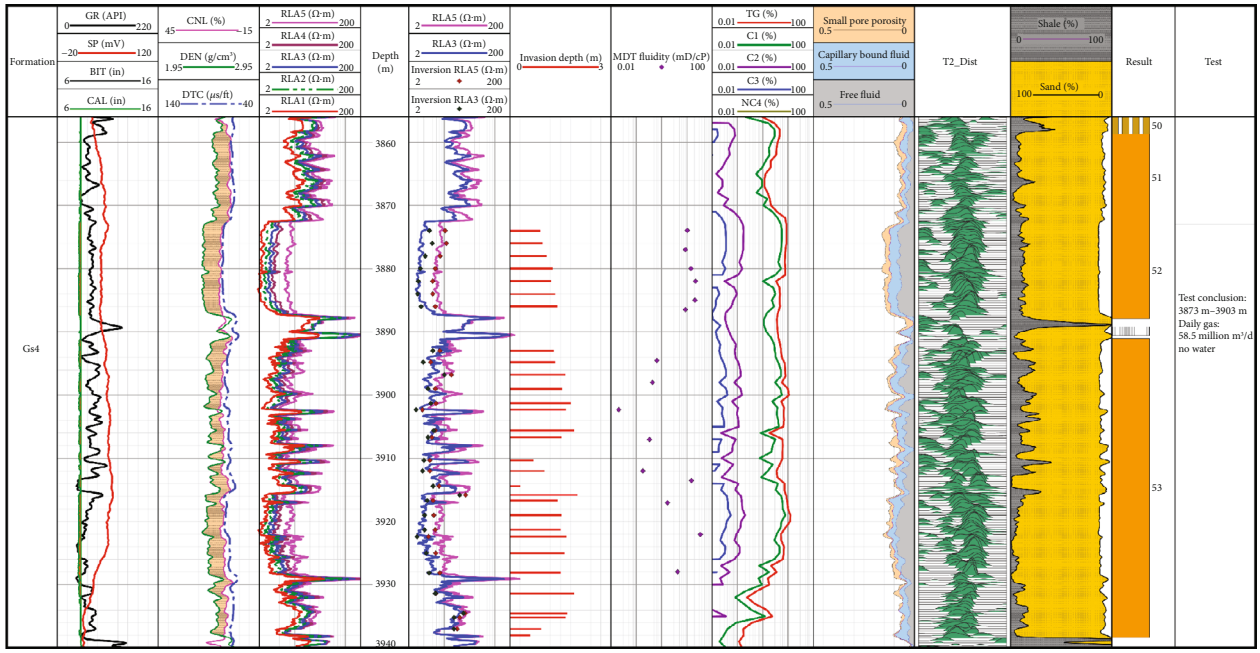

Figure 14: Log data diagram of Gs4 in X-A-3.

Table 4: Field fast water analysis data of X-A-3.

Sample sequence	Unit	Mud filtrate	3882.0 m sample	3902.3 m sample	3913.5 m sample
Sample depth	m	—	3882	3902.3	3913.5
Pumping time	min	—	315	570	735
Total anion	mg/L	59964	45957	44977	45163
Total cation	mg/L	56760	45471	39571	38576
Total salinity	mg/L	116724	91428	84548	83158
Na^+/K^+ ratio	—	1.58	1.57	1.36	1.41

the low-resistivity gas reservoir indicated that the reservoir invasion is shallow, and the influence on the electrical property is relatively weak. Accordingly, layers No. 36 and No. 37 are low-resistivity gas layers, for which the low resistivity is caused by internal factors.

5.2. External Cause. Figure 14 shows the log interpretation results of well X-A-3. A low-resistivity layer with considerable thickness appears at 3872-3930 m. According to the analysis results of water samples from three depths of 3882.0 m, 3902.3 m, and 3913.5 m (as in Table 4), the ion content exhibited no obvious difference in the three samples and the ratio of Na^+/K^+ was close to that of the mud filtrate. Analysis data showed that the three samples were mud filtrates. The five array laterolog curves all showed low apparent resistivity values, and obvious amplitude differences existed. The method mentioned in Section 4.4 was used to simulate the mud invasion of 30 sublayers. The simulation results showed that the invasion depths of some layers are greater than 1.5 m, and the inversion array laterolog values agree well with the measured values. The comprehensive analysis considers that the invasion depth is deeper than the detection range of the array laterolog, and the electric logging responses mainly reflect saline mud filtrate resistivity. The low resistivity of layers No. 52 and No. 53 is caused by the serious invasion of high salinity mud, meaning that the external factors played the leading role. This kind of low-resistivity phenomenon does not reflect the real electrical characteristics of the formation. In the calculation of petrophysical properties using the resistivity logging results, invasion correction must be considered to obtain the true formation characteristics.

5.3. Combined Cause. The resistivity of the Gs2 formation is relatively low, and the resistivity of some gas reservoirs is close to that of mudstone, such as layers No. 6 and No. 7 in Figure 15. The test data showed that the gas production is 0.65 million m^3/d with no water, and the test concluded the layers were low-resistivity gas layers. The porosity of low-resistivity formation is high (11-15%), but the permeability is relatively low (0.36-2.97 mD). The main pore radius distribution range is 0.63-2.5 μm according to the mercury injection experiment. The proportion of the small-pore porosity obtained through NMR logging data is higher than that of the gas layer below (the tenth track in Figure 15). The results showed that the complex pore structure and the large

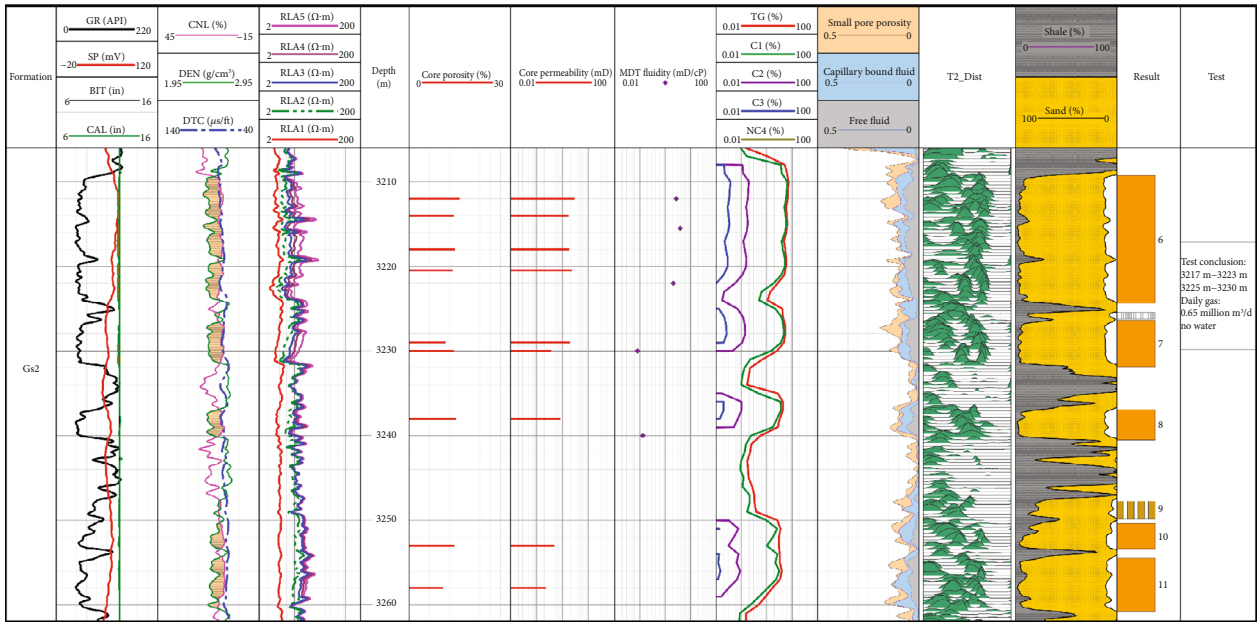

Figure 15: Log data diagram of Gs2 in X-A-1.

proportion of medium and small pores lead to the development of micropores and cause the increase of the irreducible fluid saturation. Moreover, the array laterolog curves showed obvious amplitude differences, indicating mud invasion. In conclusion, there are two reasons for the two low-resistivity gas reservoir layers. First, a relatively good conductive network is formed with the development of reservoir micropores, which enhances the conductivity of the reservoir and reduces its resistivity. Second, mud invasion occurs to a certain extent. The resistivity of the formation around the well decreases due to saline mud invasion, which causes the low response of electrical logging. Therefore, the low resistivity of these two layers is the result of the combined cause.

Most studies determine the internal causes of low resistivity by analyzing measured data such as logging and core data. It is difficult to obtain explicit evidence from the recorded data to determine the low resistivity caused by the mud invasion. In the present study, the controlling factors of low resistivity were determined by measured data coupled with numerical simulations of mud invasion. Then, the main characteristics that would lead to the generation of low resistivity were investigated and classified. In summary, the low resistivity in the reservoir may be caused by one or more reasons which can be divided into primary and secondary reasons. The electrical properties of the reservoir are affected by both internal factors and external conditions. Considering that these factors show different impacts on the resistivity logging results, the measured electrical response is generally a weighted value influenced by multiple factors simultaneously.

6. Conclusions

In the present study, for the nearly tight sandstone gas reservoir of the study area, the main controlling factors of low resistivity were determined by combining core experimental data and numerical simulation analysis of mud invasion. After all, the main conclusions would be drawn as follows:

(1) When there is no mud invasion or a low degree of mud invasion occurs

High immobile water saturation caused by the fine lithology and complex pore structure is the main factor driving the generation of low resistivity in the subject gas reservoir. The high content of clay minerals and conductive minerals such as pyrite as well as their distribution forms can considerably reduce the formation resistivity and form a low-resistivity gas reservoir.

(2) When mud invasion occurs

Invasion of the high salinity mud is the main external factor that leads to the generation of low resistivity in the gas reservoirs. For a sandstone gas reservoir, good permeability and high overbalance pressure lead to deep invasion depth. Therefore, low resistivity would be formed very easily.

(3) Case study analysis of abnormally low resistivity

Analyzing the data from the real wells revealed the main causes of abnormally low resistivity in the subject gas reservoir. It was found that the electrical response of the nearly tight sandstone gas reservoirs in this area is affected by the internal and external factors at the same time.

Considering the discussion on the detailed generation mechanism of low resistivity in gas reservoirs as presented in the current research, this study lays the foundation for selecting the optimal resistivity model for similar reservoirs.

Data Availability

The data is already included within the manuscript.

Conflicts of Interest

The authors declare that they have no conflicts of interest.

Acknowledgments

This research is supported by the Youth Science Foundation of Northeast Petroleum University (2018QNL-35).

References

[1] J. Sun, K. Wang, and J. Zhu, "Microcosmic influence factor for electrical properties of low-resistivity reservoir in Jiyang Depression," *Acta Petrolei Sinica*, vol. 27, no. 5, pp. 61–65, 2006.

[2] V. Mashaba and W. Altermann, "Calculation of water saturation in low resistivity gas reservoirs and pay-zones of the Cretaceous Grudja Formation, onshore Mozambique basin," *Marine and Petroleum Geology*, vol. 67, pp. 249–261, 2015.

[3] Z. Li, X. Cheng, H. Jiang et al., "Genetic mechanism of low-resistivity oil zones and comprehensive identification technology for well logging in the Termit Basin, Niger," *Earth Science Frontiers*, vol. 25, no. 2, pp. 99–111, 2018.

[4] R. Xie, Q. Feng, J. Gao, and G. Tao, "Mechanism of rock petrophysical parameters variations in low resistivity oil and gas reservoirs," *Chinese Journal of Geophysics*, vol. 45, no. 1, pp. 139–146, 2002.

[5] L. Yan, S. Tan, B. Pan, P. Zhang, and Y. Liu, "Genetic mechanism and logging evaluation method for low resistivity reservoirs: taking Guantao Formation of Gangbei area for instance," *Journal of Jilin University (Earth Science Edition)*, vol. 40, no. 6, pp. 1456–1462, 2010.

[6] Y. Wang, X. Song, L. He, N. Chen, and H. Yu, "Geologic origin of low-resistivity layers in deep reservoir of Gaoshangpu Oilfield," *Acta Petrolei Sinica*, vol. 31, no. 3, pp. 426–431, 2010.

[7] H. J. Hill and J. D. Milburn, "Effect of clay and water salinity on electrochemical behavior of reservoir rocks," *Transactions of AIME*, vol. 207, no. 1, pp. 65–72, 1956.

[8] M. H. Waxman and L. J. M. Smits, "Electrical conductivities in oil-bearing shaly sands," *Society of Petroleum Engineers Journal*, vol. 8, no. 2, pp. 107–122, 1968.

[9] W. W. Givens and E. J. Schmidt, "A generic electrical conduction model for low-contrast resistivity sandstones," in *SPWLA 29th Annual Logging Symposium*, San Antonio, Texas, 1988.

[10] J. Zemanek, "Low-resistivity hydrocarbon-bearing sand reservoirs," *SPE Formation Evaluation*, vol. 4, no. 4, pp. 515–521, 1989.

[11] Z. Tian, D. Bian, H. Chen, S. Ju, and W. Yan, "Application of improved PICKETT method to identification of low-resistivity pays in Y Oilfield," *Acta Petrolei Sinica*, vol. 26, no. 4, pp. 81–84, 2005.

[12] H. Yu, H. Li, B. Guo, H. Sun, and H. Zhang, "Low-resistivity oil layers fine evaluation approaches based on mechanism," *Journal of Jilin University (Earth Science Edition)*, vol. 42, no. 2, pp. 335–343, 2012.

[13] R. Chatterjee, S. D. Gupta, and M. Y. Farooqui, "Application of nuclear magnetic resonance logs for evaluating low-resistivity reservoirs: a case study from the Cambay basin, India," *Journal of Geophysics and Engineering*, vol. 9, no. 5, pp. 595–610, 2012.

[14] Z. Li, B. Zhao, Y. Guan, J. Liu, and C. Gao, "Application of nuclear magnetic resonance logging in the low-resistivity reservoir — taking the XP area as an example," *Interpretation*, vol. 8, no. 4, pp. T885–T893, 2020.

[15] N. Golsanami, E. Bakhshi, W. Yan et al., "Relationships between the geomechanical parameters and Archie's coefficients of fractured carbonate reservoirs: a new insight," *Energy Sources, Part A Recover. Util. Environ. Eff.*, pp. 1–25, 2020.

[16] N. Golsanami, X. Zhang, W. Yan et al., "NMR-based study of the pore types' contribution to the elastic response of the reservoir rock," *Energies*, vol. 14, no. 5, 2021.

[17] X. Zhou, Y. Jiang, and X. Tang, "Tectonic setting, prototype basin evolution and exploration enlightenment of Xihu sag in East China Sea basin," *China Offshore Oil Gas*, vol. 31, no. 3, pp. 1–10, 2019.

[18] X. Zhou, "Geological understanding and innovation in Xihu sag and breakthroughs in oil and gas exploration," *China Offshore Oil Gas*, vol. 32, no. 1, pp. 1–12, 2020.

[19] X. Zhou, G. Xu, H. Cui, and W. Zhang, "Fracture development and hydrocarbon accumulation in tight sandstone reservoirs of the Paleogene Huagang Formation in the central reversal tectonic belt of the Xihu Sag, East China Sea," *Petroleum Exploration and Development*, vol. 47, no. 3, pp. 462–475, 2020.

[20] Z. Zhao, C. Dong, X. Zhang et al., "Reservoir controlling factors of the Paleogene Oligocene Huagang Formation in the north central part of the Xihu Depression, East China Sea Basin, China," *Journal of Petroleum Science and Engineering*, vol. 175, pp. 159–172, 2019.

[21] F. Xu, G. Xu, Y. Liu, W. Zhang, H. Cui, and Y. Wang, "Factors controlling the development of tight sandstone reservoirs in the Huagang Formation of the central inverted structural belt in Xihu sag, East China Sea Basin," *Petroleum Exploration and Development*, vol. 47, no. 1, pp. 98–109, 2020.

[22] X. Han, J. Guo, X. Mao et al., "Definition of clay aditional conductivity intensity index for argillaceous sandstone and its application," *Chinese Journal of Geophysics*, vol. 62, no. 1, pp. 4462–4471, 2019.

[23] X. L. Sun, C. Y. Lin, X. G. Zhang et al., "Characteristics and distribution of clay minerals and their effects on reservoir quality: Huagang Formation in the Xihu Sag, East China Sea Basin," *Australian Journal of Earth Sciences*, vol. 66, no. 8, pp. 1163–1174, 2019.

[24] A. Cerepi, C. Durand, and E. Brosse, "Pore microgeometry analysis in low-resistivity sandstone reservoirs," *Journal of Petroleum Science and Engineering*, vol. 35, no. 3-4, pp. 205–232, 2002.

[25] F. Zeng, C. Dong, C. Lin et al., "Analyzing the effects of multiscale pore systems on reservoir properties–a case study on Xihu Depression, East China Sea Shelf Basin, China," *Journal of Petroleum Science and Engineering*, vol. 203, p. 108609, 2021.

[26] C. Clavier, A. Heim, and C. Scala, "Effect of pyrite on resistivity and other logging measurements," in *SPWLA 17th Annual Logging Symposium*, Denver, Colorado, 1976.

[27] M. Ben Clennell, M. Josh, L. Esteban et al., "The influence of pyrite on rock electrical properties: a case study from NW Australian gas reservoirs," in *SPWLA 51th Annual Logging Symposium*, Perth, Australia, 2010.

[28] W. W. Givens, "A conductive rock matrix model (CRMM) for the analysis of low-contrast resistivity formations," *Logic and Analysis*, vol. 28, no. 5, pp. 138–151, 1987.

[29] P. W. J. Glover, M. J. Hole, and J. Pous, "A modified Archie's law for two conducting phases," *Earth and Planetary Science Letters*, vol. 180, no. 3-4, pp. 369–383, 2000.

[30] T. Han, M. Ben Clennell, and M. Pervukhina, "Modelling the low-frequency electrical properties of pyrite-bearing reservoir sandstones," *Marine and Petroleum Geology*, vol. 68, pp. 341–351, 2015.

[31] J. T. Dewan and M. E. Chenevert, "Mudcake buildup and invasion in low permeability formations; application to permeability determination by measurement while drilling," in *SPWLA 34th Annual Logging Symposium*, Calgary, Alberta, 1993.

[32] C. Li, C. Li, C. Zhou, J. Ouyang, L. Xiu, and Y. Shi, "Effects of fresh drilling mud invasion on logging responses of dual induction and dual lateral to reservoirs," *Petroleum Exploration and Development*, vol. 34, no. 5, pp. 603–608, 2007.

[33] S. Won, H. I. Bilgesu, and S. Ameri, "Investigation of mud-filtrate invasion using computational fluid dynamics," in *SPE Eastern Regional/AAPG Eastern Section Joint Meeting*, Pittsburgh, Pennsylvania, 2008.

[34] Y. Jiang, J. Sun, J. Gao, and J. Cui, "Mud invasion and array laterolog responses in horizontal well based on numerical simulation," *Journal of Geophysics and Engineering*, vol. 14, no. 1, pp. 15–25, 2017.

[35] M. T. Galli, M. Gonfalini, M. Mele et al., "Resistivity modeling of array laterolog tools: an application in an offshore Norway clastic reservoir," *SPE Reservoir Evaluation and Engineering*, vol. 8, no. 1, pp. 77–87, 2005.

[36] H. Maurer, Y. Antonov, B. Corley, R. Khokhar, M. Rabinovich, and Z. Zhou, "Advanced processing for a new array laterolog tool," in *SPWLA 50th Annual Logging Symposium*, Woodlands, Texas, 2009.

[37] C. F. Yin, S. Z. Ke, W. Xu, M. Jiang, L. J. Zhang, and J. Tao, "3D laterolog array sonde design and response simulation," *Applied Geophysics*, vol. 11, no. 2, pp. 223–234, 2014.

[38] M. J. Nam, D. Pardo, and C. Torres-Verdín, "Simulation of DC dual-laterolog measurements in complex formations: a Fourier-series approach with nonorthogonal coordinates and self-adapting finite elements," *Geophysics*, vol. 74, no. 1, pp. E31–E43, 2009.

[39] K. Pan, W. WAng, J. Tang, and Y. Tan, "Mathematical model and fast finite element modeling of high resolution array lateral logging," *Chinese Journal of Geophysics*, vol. 56, no. 9, pp. 3197–3211, 2013.

[40] S. Deng, Z. Li, Y. Fan, and H. Chen, "Numerical simulation of mud invasion and array laterolog response in deviated wells," *Chinese Journal of Geophysics*, vol. 53, no. 4, pp. 994–1000, 2010.

[41] J. Gao, J. Sun, Q. Yu, L. Cui, and Y. Jiang, "Numerical simulation of the new sidewall array azimuthal laterolog and response characteristics," *Chinese Journal of Geophysics*, vol. 59, no. 3, pp. 1131–1142, 2016.

[42] C. Yuan, C. Li, C. Zhou et al., "Forward simulation of array laterolog resistivity in anisotropic formation and its application," *Petroleum Exploration and Development*, vol. 47, no. 1, pp. 77–85, 2020.